Check for updates

ADVANCED MATERIALS
www.advmat.de

Personal Thermoregulation by Moisture-Engineered Materials

Xiuqiang Li, Wanlin Guo, and Po-Chun Hsu**

Personal thermal management can effectively manage the skin microenvironment, improve human comfort, and reduce energy consumption. In personal thermal-management technology, owing to the high latent heat of water evaporation in wet-response textiles, heat- and moisture-transfer coexist and interact with each other. In the last few years, with rapid advances in materials science and innovative polymers, humidity-sensitive textiles have been developed for personal thermal management. However, a large gap exists between the conceptual laboratory-scale design and actual textile. Here, moisture-responsive textiles based on flap opening and closing, those based on yarn/fiber deformation, and sweat-evaporation regulation based on textile design for personal thermoregulation are reviewed, and the corresponding mechanisms and research progress are discussed. Finally, the existing engineering and scientific limitations and future developments are considered to resolve the existing issues and accelerate the practical application of moisture-responsive textiles and related technologies.

1. Introduction

The human body temperature is maintained in the range of 36.5–37.5 °C by the regulation of physiological processes such as perspiration, muscle shivering, and blood vessel constriction/dilation; hyperthermia, hypothermia, and heatstroke occur, accompanied by intense discomfort, when the body temperature is outside this range.[1,2] Traditional textiles adjust the heat and moisture balance between the human body and environment to maintain a comfortable body temperature. Thus, people often wear thick[3] or metal-coated textiles[4–6] for warmth in cold weather, whereas silk and linen fabrics with body-cooling properties, high thermal conductivity,[7,8] breathability, and softness, are preferred in hot summers.[9–15] However, the applications of traditional textiles are limited as they are unable to dynamically regulate body heating and cooling in response to environmental or metabolic heat-rate changes. To overcome this limitation, smart textiles that can switch between heating and cooling have been developed. Moreover, from the perspective of energy conservation, traditional space-heating/cooling based on heating, ventilation, and air conditioning (HVAC) consumes a large amount of energy (≈15% of the global energy consumption), causing considerable carbon dioxide emissions and global warming.[16–18] Personal thermal management focuses on the microenvironment between the textile and human body, avoiding excess indoor-space heating and cooling by HVAC, thereby reducing the energy consumption. According to Ghahramani et al.,[19] an expansion of the HVAC baseline setpoint by ±1, ±2, and ±3 °C using personal thermal management techniques could reduce HVAC energy consumption by 7.5%, 12.7%, and 16.4%, respectively. Additionally, unlike air-conditioning systems, personal thermal management enables a facile outdoor thermal-management of the human body. Therefore, smart textiles with adaptive capabilities could facilitate personal thermal management with maximum comfort and minimum energy wastage.

The human body exchanges heat with the ambient environment through textiles via three major pathways: heat conduction and convection, heat radiation, and sweat evaporation.[20–22] The working principle of smart textiles involves the adaptive tuning of heat-transfer pathways under external stimuli (such as light,[23] heat,[24] mechanical stress,[25,26] and humidity).[27] Generally, as humans use perspiration and evaporation for cooling, heat- and moisture-transfer coexist, facilitating interactions between the human body and ambient environment. Therefore, moisture management is a vital form of thermal regulation in smart textiles.

With the development of smart materials, numerous studies have focused on the design of moisture-responsive textiles. However, a substantial gap exists between the lab-scale concept

X. Li, W. Guo
Key Laboratory for Intelligent
Nano Materials and Devices of Ministry of Education
and Institute for Frontier Science
Nanjing University of Aeronautics and Astronautics
Nanjing 210016, China
E-mail: xiuqiang.li@nuaa.edu.cn
P.-C. Hsu
Pritzker School of Molecular Engineering
University of Chicago
Chicago, IL 60637, USA
E-mail: pochun.hsu@duke.edu

The ORCID identification number(s) for the author(s) of this article can be found under https://doi.org/10.1002/adma.202209825

© 2023 The Authors. Advanced Materials published by Wiley-VCH GmbH. This is an open access article under the terms of the Creative Commons Attribution-NonCommercial-NoDerivs License, which permits use and distribution in any medium, provided the original work is properly cited, the use is non-commercial and no modifications or adaptations are made.

DOI: 10.1002/adma.202209825

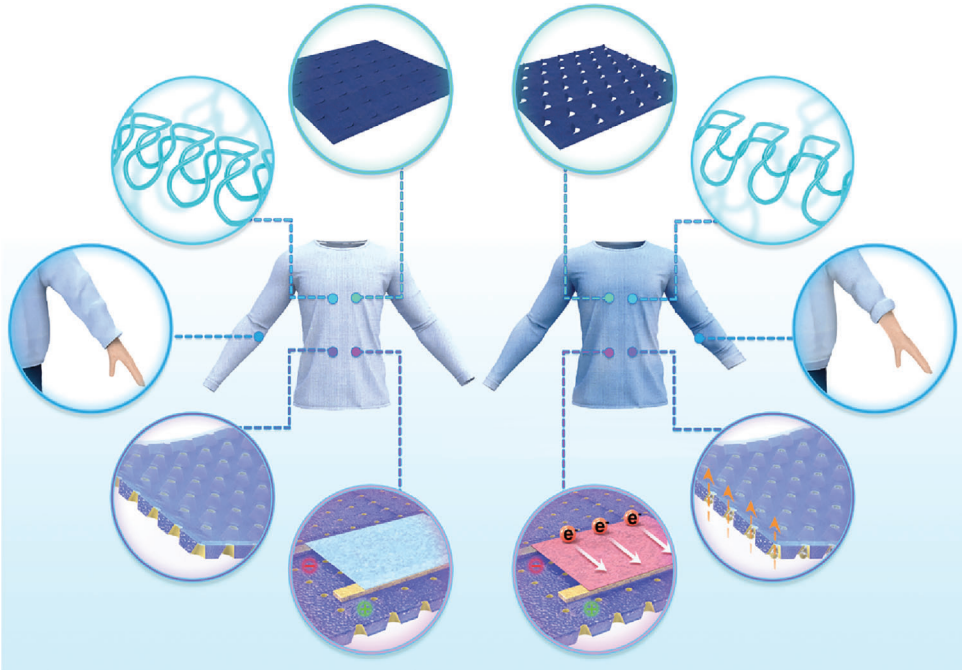

Figure 1. Schematic illustration of personal thermoregulation by moisture-engineered materials.

designs and practical textiles. To fabricate moisture-responsive textiles with acceptable repeatability, stability, washability, and aesthetics, the material and device-structure designs require improvement. To facilitate the development of such textiles with real-life applications, as shown in **Figure 1**, their moisture-responsive behavior has been classified into three categories. First, moisture response based on flap opening and closing. Second, response based on yarn/fiber deformation (including interyarn/fiber spacing and textile length regulation). Third, textile-design induced sweat-evaporation regulation for personal thermoregulation (with/without power generation). Here, the principles, current progress, and bottlenecks encountered in the development of moisture-responsive textiles have been summarized. Additionally, the outlooks are discussed at the end of the paper. This review paper could guide future research on moisture-responsive textiles and facilitate their utilization in personal thermal management, wearable devices, and the water-energy nexus.

2. Model

A previous publication describes a 1D steady-state model to elucidate the heat and mass transfer processes during the evaporative cooling of textiles.[28] This model can be used to understand the textile components in detail and improve their design. As shown in **Figure 2**, the steady-state energy balance in the system can be expressed by the following equation:

$$q''_{\text{eva}} = q''_{\text{body}} + q''_{\text{conv}} + q''_{\text{rad}} + q''_{\text{solar}} \tag{1}$$

The body-cooling heat flux can be expressed by the following:

$$q''_{\text{body}} = \frac{T_{\text{core}} - T_{\text{eva}}}{R} = \frac{T_{\text{core}} - T_{\text{eva}}}{\frac{L_{\text{fat}}}{k_{\text{fat}}} + \frac{L_{\text{skin}}}{k_{\text{skin}}} + \frac{L_{\text{vest}}}{k_{\text{water}}}} \tag{2}$$

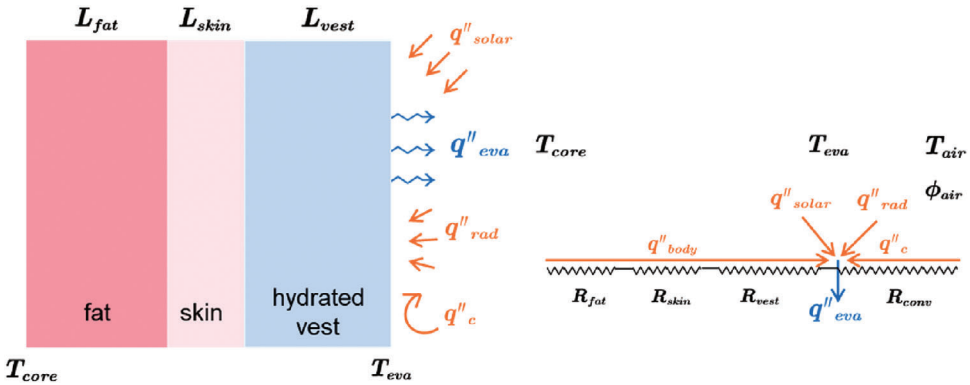

Figure 2. Heat and mass transfer processes and the thermal resistance network in the evaporative cooling of textiles.

© 2023 The Authors. Advanced Materials published by Wiley-VCH GmbH

15214095, 0, Downloaded from https://onlinelibrary.wiley.com/doi/10.1002/adma.202209825 by University Of Chicago Library, Wiley Online Library on [25/07/2023]. See the Terms and Conditions (https://onlinelibrary.wiley.com/terms-and-conditions) on Wiley Online Library for rules of use; OA articles are governed by the applicable Creative Commons License

where T_{core} and T_{eva} represent the body core and evaporative textile-surface temperature, respectively. The convective heat flux can be calculated by the following:

$$q''_{body} = h_c \left(T_{air} - T_{eva}\right) \tag{3}$$

where h_c is related to the air velocity ($h_{conv} = 8.1v^{0.5}$).

The evaporative heat flux can be calculated by the following:

$$q''_{body} = h_{eva} \left(P_{w,eva}\left(T_{eva}\right) - P_{w,air}\left(T_{air}, \varphi_{air}\right)\right) = C_L h_c \left(P_{w,eva} - P_{w,air}\right) \tag{4}$$

where h_{eva} is the evaporative heat-transfer coefficient, which can be calculated using Lewis' relation, $h_{eva} \approx C_L h_c \approx 0.0168 h_c$. $P_{w,air}$ and $P_{w,eva}$ are the partial pressures of water in air and on the surface of the evaporating textile, respectively. For a given T_{air} and Φ_{air}, the partial pressure of water (P_a) can be calculated by the following:

$$P_{w,air}\left(T_{air}, \varphi_{air}\right) = 133.3\varphi_{air} e^{20.386 - \frac{5132}{273 + T_{air}}} \tag{5}$$

Consequently, the portion of solar radiation that can directly affect the wearer, expressed by the clear-sky index, sk_t, is ≈0.8 (the diffuse-reflection portion, sk_d, is ≈0.2). For a given solar zenith angle, θ_z, the clear-sky solar radiation, I_g, in the horizontal plane can be calculated by the following:

$$I_g = 1098 \cos\theta_z e^{\frac{-0.057}{\cos\theta_z}} \tag{6}$$

For simplicity, the following linear formula for radiative heat exchange is often used to analyze the body-temperature control within an enclosure:

$$q''_{rad} = h_{rad}\left(T_{air} - T_{rad}\right) \tag{7}$$

where h_{rad} is the radiative heat-transfer coefficient (4.5 W m^{-2} °C^{-1} is the typical value for most body parts). Substituting equations (A2)–(A7) into Equation (1), the resulting expression for T_{eva} is:

$$T_{eva} = \frac{-0.0168 h_c \left(P_{w,eva}\left(T_{eva}\right) - P_{w,air}\left(T_{air}, \varphi_{air}\right)\right) + \frac{T_{core}}{R} + T_{air}\left(h_c + h_{rad}\right) + \alpha_T q''_{solar}}{h_c + h_{rad} + \frac{1}{R}} \tag{8}$$

3. Moisture-Responsive Textiles for Personal Thermoregulation

3.1. Moisture-Responsive Textiles Based on Flap Opening and Closing

As the diffusion of water vapor in a hygroscopic material is a heterogeneous process along the thickness direction, it generates a humidity gradient in the material. This causes the upper and lower surfaces of the hygroscopic material to expand differently (moisture absorption often causes a volume expansion of the hygroscopic material), showing the characteristics of curling. A category of moisture-responsive textiles is based on this principle; they enable thermal moisture management by the opening and closing of numerous flaps under wet and dry states on hygroscopic materials,[29–36] including Nafion,[29,30] microbial cells,[31] and nylon[32] (**Table 1**). In a cold environment (under dry conditions), the flaps are closed to suppress thermal convection/heat conduction and thermal radiation between the human body and ambient environment for warming. Conversely, when the human body is sweating (under wet conditions), the flaps open (curling) to promote thermal convection and conduction, heat radiation, and sweat evaporation for cooling.

Zhong et al.[29] have reported a hygroscopic Nafion-polymer moisture-responsive textile that functions by flap opening and closing (**Figure 3**a); its polymeric chains contain a hydrophobic poly(tetrafluoroethylene) backbone and hydrophilic perfluoroether sulfonic acid side chains (–SO_3H). On exposure to water vapor, H^+ undergoes exchange with water, forming numerous water-transport microchannels; this separates the hydrophobic and hydrophilic domains, causing a swelling effect (Figure 3b). Subsequently, on releasing water, the polymer regains its original state. Experimental results indicate that the flaps open at a humidity of 86.8% (after 40 s), causing a 1.1 °C temperature-drop in the textile, until the flaps close at a humidity of 83.4%. After sweating, the textile exhibits a temperature-drop of up to 1.55 °C (Figure 3c), causing a distinct cooling effect on the human body. Mu et al.[30] have reported a perfluorosulfonic acid ionomer (PFSA, otherwise known as Nafion) moisture-responsive material with the same principle of expansion (Figure 3d). The PFSA material exhibits the properties of a moisture-responsive actuator; 75 µm single-layer PFSA films show a rapid response speed (0.25 s) and high stability (>8000 cycles without deterioration) under 18% ethanol-vapor atmosphere. Additionally, as shown in Figure 3e, the authors have constructed a kirigami-inspired single-layer actuator system for human thermal management using laser cutting and patterning. An analysis of the skin temperature of a man wearing a PFSA actuator-based shirt after running 3 km indicates that wearing the new textile causes a 1.3 °C-lower skin temperature than wearing traditional textiles under similar conditions; this could be attributed to accelerated heat exchange between the human body and external environment due to flap opening in the textile-material (Figure 3f).

Subsequently, materials with better performance and practicality than Nafion films have been designed, and significant progress has been made in combining devices and textiles, while maintaining aesthetics and practicality. Wang et al.[31] have reported a hygroscopic material (microbial cells) that changes its specific volume on altering the surrounding-water activity. Sandwich-structure microbial cells/moisture-inert material/microbial cells systems have been designed for moisture-responsive textiles to confirm the reversible shape transformation of microbial cells (**Figure 4**a). Additionally, a running suit with back ventilation based on the sweat and

© 2023 The Authors. Advanced Materials published by Wiley-VCH GmbH

15214095, 0, Downloaded from https://onlinelibrary.wiley.com/doi/10.1002/adma.202209825 by University Of Chicago Library, Wiley Online Library on [25/07/2023]. See the Terms and Conditions (https://onlinelibrary.wiley.com/terms-and-conditions) on Wiley Online Library for rules of use; OA articles are governed by the applicable Creative Commons License

Table 1. Summary and comparison of moisture-responsive textiles based on flap opening and closing reported in the literature.

	Materials	Radiation: low emissivity for heating	Radiation: high emissivity for cooling	Color design	Thermal management performances
Zhong et al.[29]	Nafion	×	√	×	Exhibits a maximum temperature reduction of 1.55 °C.
Mu et al.[30]	Nafion	×	√	√	The temperature of a runner's skin is 1.3 °C lower than that of traditional textiles.
Wang et al.[31]	Biohybrid film	×	√	×	Generates a 2 °C lower temperature reduction compared to traditional cloth.
Li et al.[32]	Metallized nylon	√	√	√	Multimodal adaptive textiles expand the thermal comfort zone 30.7% and 20.7% more than traditional static textiles and single-modal adaptive wearables, respectively.
Kapsali et al.[33]	Woven polyester/polymeric adhesives/polyether-ester block copolymer membrane	×	√	×	–
Kim et al.[34]	Poly(ethylene glycol) and cellulose acetate/polyester-type polymer	×	√	×	After flap opening, smart textiles exhibit 6 °C-lower maximum cooling compared to normal textiles.
Yang et al.[35]	Natural fibers	×	√	×	–
Zhao et al.[36]	MXene-modified polyamide filament/polypropylene	×	√	×	With smart textiles, the skin temperature is ≈1 °C lower than with the control.

heat maps of the human body has been fabricated (Figure 4b). On exercising for 5 min, subjects begin to perspire; unlike traditional cloth, flaps in the new textile automatically open for effective sweat evaporation, cooling the microenvironment between the skin and textile, and generating a temperature drop of ≈2 °C (Figure 4c). Similarly, as shown in Figure 4d,e, Kapsali et al.[33] have reported a moisture-responsive textile composed of a tightly woven polyester and hydrophilic polyether-ester block-copolymer membrane connected by hydrophilic polymeric adhesives. Under moisture, the polyester fibers swell slightly,

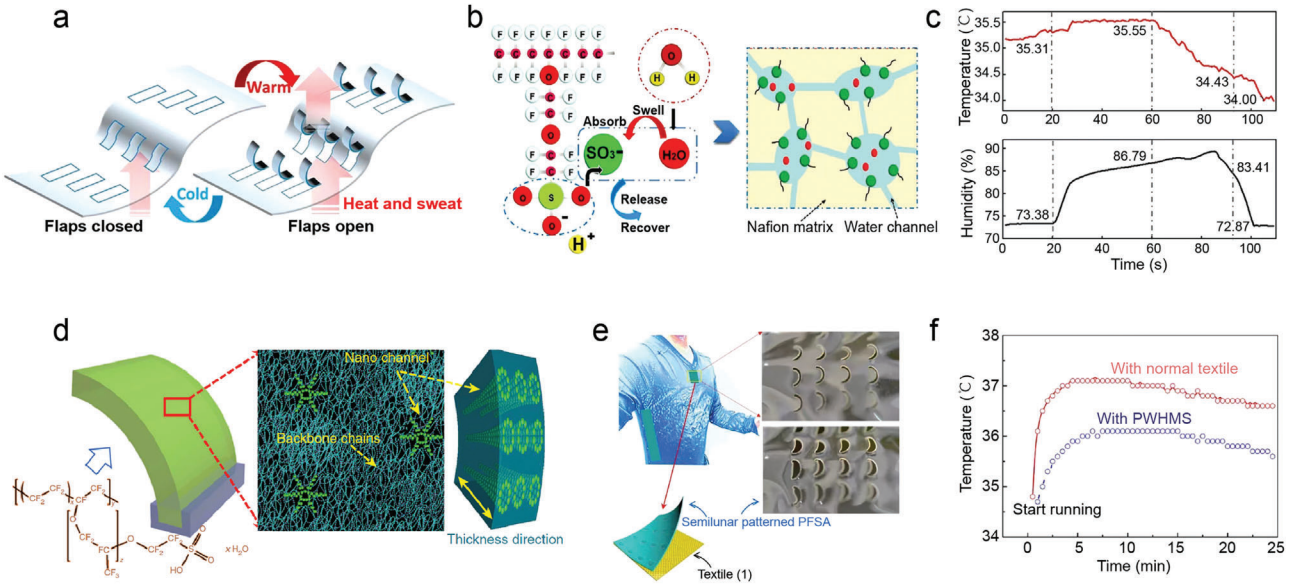

Figure 3. a) Schematic diagram of a moisture-responsive Nafion sheet with openable flaps that mimics the thermal-adaptation function of human skin. b) Mechanisms of swelling and water transport in Nafion. c) Temperature and moisture-responsive behavior of a "sweating" skin-simulation system at 35 °C. a–c) Reproduced with permission.[29] Copyright 2017, Springer Nature. d) Chemical structure and microstructure of the molecular channel distribution of PSFA. e) A PFSA matrix with a half-moon pattern used in commercial sportswear for personal thermal-moisture management. f) Skin temperature over time with different textiles. d–f) Reproduced with permission.[30] Copyright 2018, Springer Nature.

 © 2023 The Authors. Advanced Materials published by Wiley-VCH GmbH

15214095, 0, Downloaded from https://onlinelibrary.wiley.com/doi/10.1002/adma.202209825 by University Of Chicago Library, Wiley Online Library on [25/07/2023]. See the Terms and Conditions (https://onlinelibrary.wiley.com/terms-and-conditions) on Wiley Online Library for rules of use; OA articles are governed by the applicable Creative Commons License

while the polyether component swells significantly, facilitating flap opening. Based on this, Nike have developed a knitted textile (named Micro React) consisting of two layers (a hydrophobic polyester-fiber upper layer and a lower layer composed of hydrophilic polyamide fiber-based yarns). A flower-shaped pattern composed of several flaps was designed based on this material, and has been used in a tennis dress to regulate the human body temperature.

Although a series of moisture-responsive materials with good performance has been reported, their tuning mechanisms are solely based on thermal convection and conduction. As textiles and human skin are both high mid-infrared (IR) emitters, flap switching does not cause emission regulation; it accounts for ≈50% of the heat dissipation from the human body under typical indoor conditions, significantly limiting the thermal-management performance of moisture-responsive textiles. A significantly greater tuning range is facilitated by the coordination of multiple heat-transfer mechanisms. Therefore, a three-layer structure with polystyrene-*block*-poly(ethylene-*ran*-butylene)-*block*-polystyrene (SEBS) nanocomposite, metal, and nylon 6 layers (**Figure 5**a and 5b)[32] has been constructed. Similar to other hygroscopic materials, the absorption and release of water vapor by nylon-6 regulates flap-opening and -closing; the expansion/contraction principles are shown in Figure 5b. Although the metal layer shows a clamping effect on nylon 6, improving its moisture-responsive performance, it causes a lower emissivity of the outer surface of the textile. SEBS nanocomposites form color layers (different from traditional-dye color layers) with high mid-IR emissivity that enhance the aesthetics of smart textiles to meet practical applications. These color layers are designed to exhibit high mid-IR transparency to ensure no influence of coloration on their emission tunability. Thermal regulation by these materials occurs as described previously (similar to other moisture-responsive materials) when the flaps are open, while the textile suppresses heat conduction, convection, and radiation when the flaps are closed, enabling good thermal management (Figure 5a). For this textile, the coordinated regulation of multiple heat-transfer mechanisms improves its heating management by 16.3% under dry conditions and cooling management by 14.4% under wet conditions, expanding the thermal comfort zone by 30.7% compared to traditional textiles (Figure 5c). Outdoor experimentation with this new textile (attached to the back of a commercial T-shirt) indicates that all the textile-flaps open to promote heat dissipation when the subject wearing the modified T-shirt exercises for 5 min, and the flaps close when the subject stops exercising (to allow sweat evaporation).

3.2. Moisture-Responsive Textiles Based on Yarn/Fiber Deformation

3.2.1. Regulation of Interyarn/Fiber Spacing

Moisture-responsive textiles based on yarn/fiber deformation that involve interyarn/fiber-spacing and textile-length tuning have been used for thermal regulation. Currently, interyarn/fiber-spacing regulation is based on two principles: competing hydrophobic and hydrophilic effects[37,38] and molecular-chain stretching during hydration and dehydration.[39,40] Increasing the interyarn/fiber spacing (under wet conditions) has a cooling effect as it enhances the convection/conduction and radiation of heat, along with sweat evaporation from the human body, while a reduction of interyarn/fiber spacing (under dry conditions) has a heating effect due to the suppression of heat transfer (**Table 2**).

Based on the principle of competing hydrophobicity and hydrophilicity (**Figure 6**a,b), Zhang et al.[37] have designed

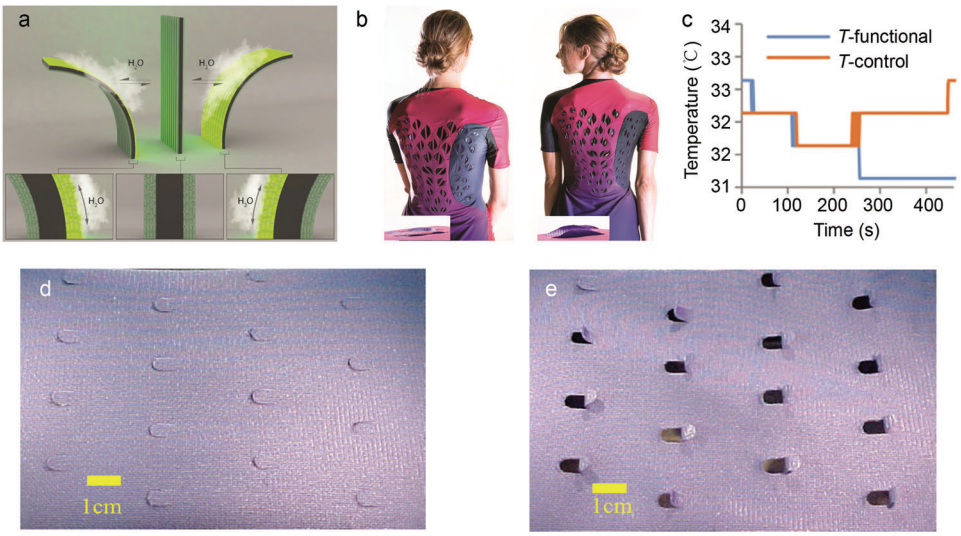

Figure 4. a) Shape transformation of films with the microbial cells/moisture-inert materials/microbial cells sandwich-structure material on exposure to moisture. b) Images of the flat ventilation flap of the clothing prototype before exercise and curved ventilation flap after exercise. c) Temperature curves of the stagnant air layer near the skin of a volunteer wearing clothing with (blue) and without (orange) flaps. a–c) Adapted with permission.[31] Copyright 2017, American Association for the Advancement of Science. d,e) Photographs of polyester fibers with flaps under dry (d) and moist (e) conditions. d,e) Reproduced with permission.[33] Copyright 2020, MDPI.

© 2023 The Authors. Advanced Materials published by Wiley-VCH GmbH

15214095, 0, Downloaded from https://onlinelibrary.wiley.com/doi/10.1002/adma.202209825 by University Of Chicago Library, Wiley Online Library on [25/07/2023]. See the Terms and Conditions (https://onlinelibrary.wiley.com/terms-and-conditions) on Wiley Online Library for rules of use; OA articles are governed by the applicable Creative Commons License

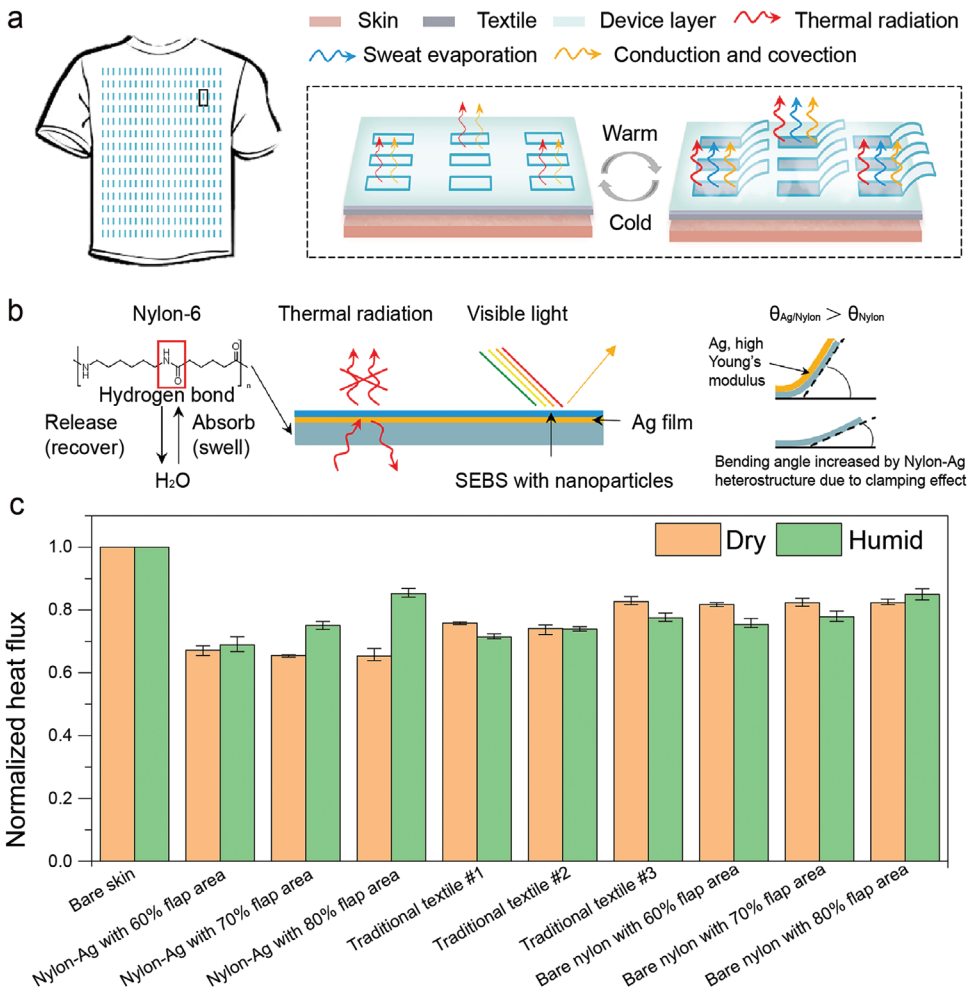

Figure 5. a) Working principle of multimodal wearable devices based on nylon/silver heterostructures. b) Configuration of the nylon-Ag-SEBS heterostructure and functional scheme of each layer. c) Normalized heat fluxes of different types of textiles/wearable devices in the dry and humid states. a–c) Reproduced with permission.[32] Copyright 2021, American Association for the Advancement of Science.

few-walled carbon nanotube (CNT)-coated triacetate-cellulose side-by-side bimorph fibers with interyarn/fiber spacing regulation through moisture responsiveness. Under wet conditions (open), the yarn collapses (an unbalanced expansion of cellulose (hydrophilic)-triacetate (hydrophobic) causes fiber mechanical actuation within the knitted textile), increasing the proximity of the fiber metaelements (CNTs) and inducing resonant electromagnetic coupling, to enhance the thermal radiation of the human body, facilitating heat dissipation. Conversely, under dry conditions (close), the yarn suppresses heat dissipation. Textile switching between the wet and dry conditions (Figure 6b) causes >35% IR modulation. Fu et al.[38] have reported a knitted textile composed of hydrophilic cellulose fibers and hydrophobic polyethylene terephthalate. In the wet state, the interyarn spacing increases (from a densely packed state to a loose state) due to fiber deformation caused by the unbalanced expansion of cellulose fibers and polyethylene terephthalate, promoting heat exchange between the human body and ambient environment (Figure 6c,d). Thus, the IR transmittance of the designed textile is ≈2 times and its transmittance in the dry state is ≈8 times that of conventional textiles under wet conditions. Moreover, unlike traditional textiles, on changing its porosity from 10% to 47%, its heat flux increases from 74.4 to 152.3 W cm^{-2}, and its cooling effect increases by 105%.

Based on molecular-chain stretching during hydration and dehydration, Hu et al.[39] have designed a moisture-responsive knitted textile using 100% descaled wool yarn. Water absorption increases the length of the woolen yarn and decreases its diameter, increasing the interyarn spacing (**Figure 7**a–c); this molecular-chain expansion is possibly due to an increase in molecular vibrations along the woolen-yarn chains on water absorption. The wool regains its original state on the loss of water, keeping it warm. The textile porosity increases by 70% at 100% water absorption, and the air permeability increases by >60%. Additionally, the IR transmittance is higher in the wet state (9.6–10 μm) than in the dry state (Figure 7c). IR temperature measurements indicate that the surface temperature of the textile in the wet state (24.7 °C) is significantly lower than in the dry state (31.2 °C) (Figure 7b). Subsequently, Iqbal et al.[40] have analyzed the water-responsive switch ability of different wool-textile architectures. A compari-

© 2023 The Authors. Advanced Materials published by Wiley-VCH GmbH

15214095, 0, Downloaded from https://onlinelibrary.wiley.com/doi/10.1002/adma.202209825 by University Of Chicago Library, Wiley Online Library on [25/07/2023]. See the Terms and Conditions (https://onlinelibrary.wiley.com/terms-and-conditions) on Wiley Online Library for rules of use; OA articles are governed by the applicable Creative Commons License

Table 2. Summary and comparison of moisture-responsive textiles based on yarn/fiber deformation reported in the literature.

	Materials	Tuning method	Material/device responsiveness	Thermal management performances
Zhang et al.[37]	Bimorph fibers with carbon nanotubes	Regulation of interyarn/fiber spacing	>35% IR can be tuned as the relative humidity of the underlying is skin changed.	-
Fu et al.[38]	Hydrophobic poly(ethylene terephthalate) and hydrophilic cellulose fibers	Regulation of interyarn/fiber spacing	IR transmittance of the designed textile is ≈2 times greater in the dry state and ≈8 times greater in the wet state compared to that of conventional cotton textiles.	Cooling effect of the textile is 105% greater than that of commercial cotton textiles.
Hu et al.[39]	Wool	Regulation of interyarn/fiber spacing	Porosity of the textile is increased by 70% at 100% water absorption, and its air permeability is increased by more than 60%.	The textile surface-temperature in the wet state (24.7 °C) is significantly lower than in the dry state (31.2 °C).
Iqbal et al.[40]	Wool	Regulation of interyarn/fiber spacing	Air permeability, conductive heat loss, and cool-touch feeling of single jerseys in the wet state are 30, 50, and 50% higher than those of a double-knit structure.	No specific value given.
Jia et al.[47]	Silk	Textile length regulation	On exposure to water fog, the torsional silk fiber exhibits a reversible torsional stroke of 547° mm^{-1}.	It exhibits 70% contraction on increasing the humidity from 20% to 80%.
Yin et al.[48]	Silk	Textile length regulation	The wetting/drying process in response to water and ethanol requires approximately 125 and 22 s, respectively.	–
Hu et al.[49]	Bamboo	Textile length regulation	The twisted actuator exhibits a torsional actuation of 64.4° mm^{-1} in 4.2 s. It causes 50% contraction in a coiled tensile actuator.	–
Leng et al.[50]	Hair	Textile length regulation	Homochiral- and heterochiral-fiber artificial muscles show 94% contraction and 3000% elongation, and a maximum work capacity of 6.35 J kg^{-1} and energy density of 69.8 kJ m^{-3} under	–
Peng et al.[51]	Viscose fiber-based artificial muscles	Textile length regulation	They exhibit a reversible torsional stroke of 1752° cm^{-1} with a maximum rotational speed of 2100 rpm.	–
Wanget al.[52]	Lotus-fiber yarn artificial muscles	Textile length regulation	They exhibit a reversible muscle-length torsional stroke of 200° mm and 200 rpm peak rotation speed. A 2.5 cm long muscle generates a specific torque of 488 mN m kg^{-1}.	–

son of single unbalanced jersey with balanced double-knit materials indicates that single-jersey loop shapes exhibit more facile alteration than double-knit textiles. Thus, the air permeability, conductive heat loss, and cool-touch feeling of single jerseys in the wet state are 30%, 50%, and 50% higher than those of double-knit structures, respectively. Additionally, single jersey samples exhibit better water-vapor transmission, radiative heat loss under dry and wet conditions, evaporation rates, and wicking distances than double-knit structures.

3.2.2. Textile-Length Regulation

An interesting mechanism of yarn/fiber deformation involves textile-length regulation through "artificial muscles",[41–46] particularly moisture-responsive "artificial muscles". The artificial-muscle response mechanism usually involves volume expansion after water absorption, with fiber tensile and torsional actions caused (and/or enhanced) by twisting, coiling, and plying. The textile adaptively adjusts its length with humidity, similar to dressing and undressing, for personal thermoregulation.

To date, artificial muscles based on natural fibers (silk,[47,48] bamboo,[49] hair[50]), viscose fibers,[51] and lotus fiber yarns[52] have been developed for moisture-responsive textiles. Jia et al.[47] have reported moisture-responsive textiles containing silk-fiber artificial muscles with a torque-balanced two-ply structure to avoid twist release (**Figure 8**a). Silk proteins show a disruption of hydrogen bonding after moisture absorption, causing a transformation of the silk structure with reversible expansion and contraction. On contacting with water vapor, the textile exhibits a reversible torsional stroke of 547° mm^{-1}, with 70% contraction on increasing the humidity from 20% to 80%. Experimentation with a skirt fabricated to demonstrate the moisture-responsive performance of the textile indicates 45% contraction in the wet state (for accelerated body-heat dissipation), and a return to the original state under dry-body conditions (Figure 8b). Peng et al.[51] have reported a viscose-fiber-based artificial muscle with a hierarchical structure for use in moisture-responsive textiles. As shown in

© 2023 The Authors. Advanced Materials published by Wiley-VCH GmbH

15214095, 0, Downloaded from https://onlinelibrary.wiley.com/doi/10.1002/adma.202209825 by University Of Chicago Library, Wiley Online Library on [25/07/2023]. See the Terms and Conditions (https://onlinelibrary.wiley.com/terms-and-conditions) on Wiley Online Library for rules of use; OA articles are governed by the applicable Creative Commons License

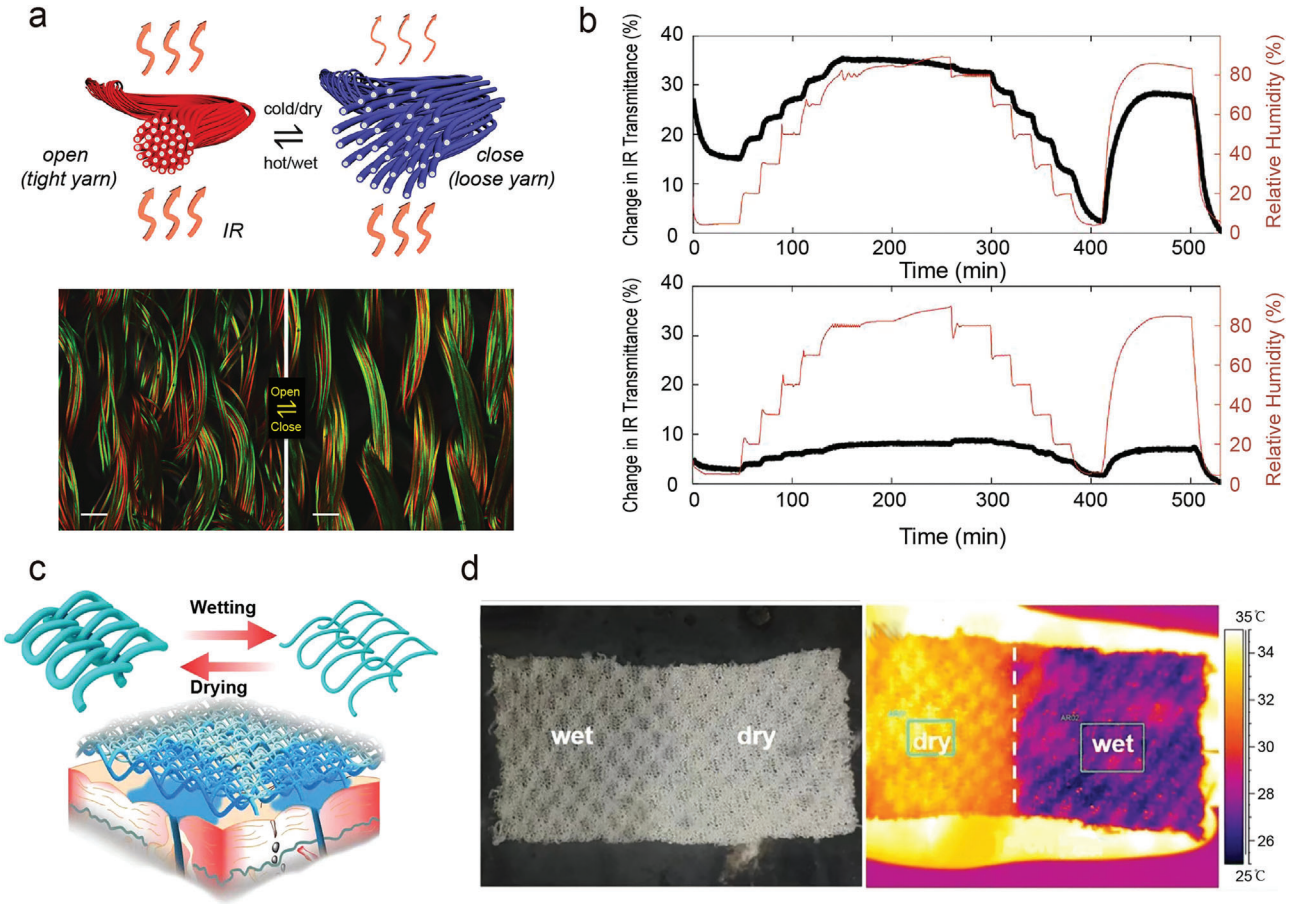

Figure 6. a) Schematic diagram and confocal fluorescence microscopy images of knitted textiles in the closed (low moisture) and open (high moisture) states. b) IR-transmittance variation (black line) with relative humidity for metatextiles (above) and traditional textiles (below). a,b) Reproduced with permission.[37] Copyright 2019, American Association for the Advancement of Science. c) Schematic diagram of the reversible loop-structure change during wetting and drying. d) Dry and wet sections of the cooling textile. IR images of the dry and wet areas of the cooling textile kept on a palm. c,d) Reproduced with permission.[38] Copyright 2019, Springer Nature.

Figure 8c, the alignment of the fiber microstructure is enhanced through the hot-drawing process, and a double-helical yarn is designed by twisting and plying. Moisture absorption disrupts hydrogen bonding in the structure and reduces the fiber length; on drying, the fiber regains its original length (due to dehydration and the re-formation of hydrogen bonds). Benefiting from the cross-scale processing strategy (Figure 8c), the structure exhibits a reversible torsional stroke of 1752° cm^{-1}, with a maximum rotational speed of up to 2100 rpm. Knitwear has been fabricated based on this material; its sleeves automatically roll-up in the wet state to enhance heat dissipation from the body, while they are automatically lowered to keep the human body warm under dry conditions (Figure 8d).

4. Sweat-Evaporation Regulation by Textile Design for Personal Thermoregulation

The directional transport of sweat is challenging in traditional textiles due to their symmetrical wettability and inner- and outer-surface structures. To create a comfortable microenvironment for the human body, it is vital to suppress wet adhesion. Numerous studies on smart textiles have focused on directional sweat transport through anisotropic design for a quick-drying effect on the skin through sweat transport from the skin to the ambient atmosphere;[53–62] this process is often accompanied by sweat evaporation (i.e., heat transfer). Some studies have reported the development of smart textiles with directional sweat transport and thermal management functions.[63–69] This review focuses on the combination of directional sweat transport and personal thermal management through textile design (**Table 3**). The mechanism, materials, and preparation methods for directional sweat transport can be found in ref. [54].

Dai et al.[63] have reported a hydrophobic/superhydrophilic Janus polyester (PE)/nitrocellulose (NC) textile; embedded conical micropore arrays with hydrophilic inner walls rapidly pump sweat to its superhydrophilic NC layer (driven by capillary forces) for directional sweat transport (**Figure 9**a). This textile exhibits a directional transport index of 1246%, and the temperature of cotton textile-covered areas (≈21.7 °C) is 2.6 °C lower than areas covered by the Janus PE/NC textile (≈24.3 °C) under wet conditions (Figure 9b), possibly due to the lower thermal conductivity of the PE/NC textile under wet conditions, which causes a

© 2023 The Authors. Advanced Materials published by Wiley-VCH GmbH

15214095, 0, Downloaded from https://onlinelibrary.wiley.com/doi/10.1002/adma.202209825 by University Of Chicago Library, Wiley Online Library on [25/07/2023]. See the Terms and Conditions (https://onlinelibrary.wiley.com/terms-and-conditions) on Wiley Online Library for rules of use; OA articles are governed by the applicable Creative Commons License

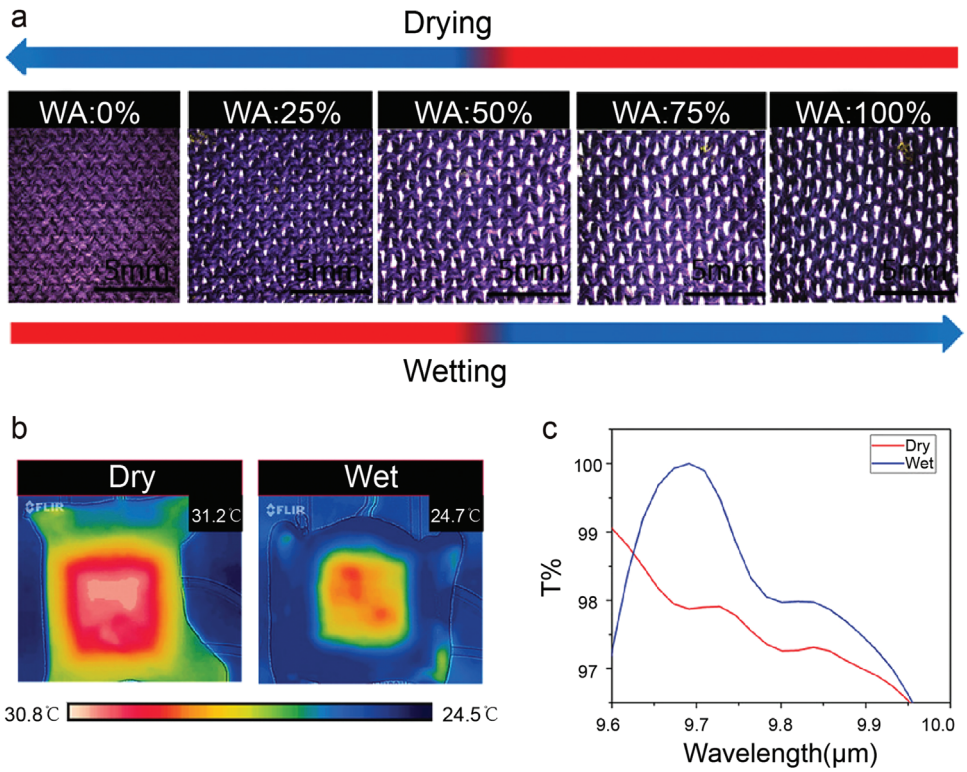

Figure 7. a) Light microscopy pictures of pore openings in knitted woolen textiles with increasing water absorption (backing layer). b) Thermal images of woolen textiles under dry and wet conditions. c) IR transmittance through dry and wet knitted-wool textiles. a–c) Reproduced with permission.[39] Copyright 2020, Wiley-VCH.

warmer sensation than cotton. In a follow-up study, Miao et al.[64] and Peng et al.[65] have reported textiles with optimized thermal properties for efficient personal drying and cooling. Miao et al.[64] have developed a biomimetic transpiration textile with decreasing capillary pore sizes and aligned polyurethane (PU)/boron nitride nanosheet (BNNS) fibers to simulate vascular and mesophyll tissues for directional sweat transport (Figure 9c). The thermal conductivity of BNNS is enhanced in the textile, which exhibits 0.182 and 1.137 W m^{-1} K^{-1} thermal conductivity in the cross-plane and in-plane directions, respectively. Moreover, the aligned PU/BNNS fibers crossing each other shorten the heat-transfer paths and reduce the interfacial thermal resistance. Consequently, the structure exhibits a one-way water-transport index of 1072%, with an evaporation rate of 0.36 g h^{-1}. Due to excellent thermal design, the PU/BNNS fabrics exhibit high surface temperatures under dry and wet conditions, with efficient heat dissipation (Figure 9d). Interestingly, the two aforementioned publications report opposite conclusions. According to one study, the high surface temperature is due to the low thermal conductivity of the material; contrarily, the other study reports that it is due to the high thermal conductivity of the material. As the surface temperature is also related to the evaporation rate of the material, this mechanism requires further investigation. Peng et al.[65] have proposed an integrated cooling (i-Cool) textile for personal thermal moisture management. In i-Cool textiles, the original high-thermal-conductivity textile with holes is used as the matrix, while hole-cellulose forms water-transport channels for rapid heat and sweat transfer (**Figure 10**a,b). Moreover, a thermal test device has been constructed to simulate the skin environment and determine the relationship between the skin temperature and textile sweating-rate (Figure 10c). In the steady-state evaporation test, the skin power density increases by ≈3 times compared to cotton textiles, with over 100% reduction in the water mass-gain ratio (water mass gain/textile sample dry mass × 100%). Additionally, i-Cool textiles show a cooling effect of ≈3 °C in the artificial sweating-skin test, while consuming less sweat than cotton.

Hu et al.[67] have combined rapid water transportation/evaporation with radiative cooling. The reported textile enables thermal management of the human body while sweating, and radiative cooling in the absence of sweating. The authors have designed bilayer nanoporous polyethylene membranes with anisotropic wettability exhibiting temperatures that are ≈2.6 °C lower than those exhibited by cotton textiles through radiative cooling without sweating. Owing to efficient sweat transport and evaporation cooling, the textile exhibits temperatures that are ≈1.0 °C lower than those shown by cotton textiles during sweating, and it reduces sticking.

Thus, heterostructure and evaporation design facilitates the directional transmission of sweat and cooling; however, the aforementioned design does not exhibit efficient heating regulation. For dynamic heating and cooling regulation, as shown in Figure 10d, Wang et al.[67] have designed a temperature-responsive Janus textile enabling reversible one-way water transportation and adaptive heat and moisture management. This textile is composed of two temperature-responsive polymers,

© 2023 The Authors. Advanced Materials published by Wiley-VCH GmbH

15214095, 0, Downloaded from https://onlinelibrary.wiley.com/doi/10.1002/adma.202209825 by University Of Chicago Library, Wiley Online Library on [25/07/2023]. See the Terms and Conditions (https://onlinelibrary.wiley.com/terms-and-conditions) on Wiley Online Library for rules of use; OA articles are governed by the applicable Creative Commons License

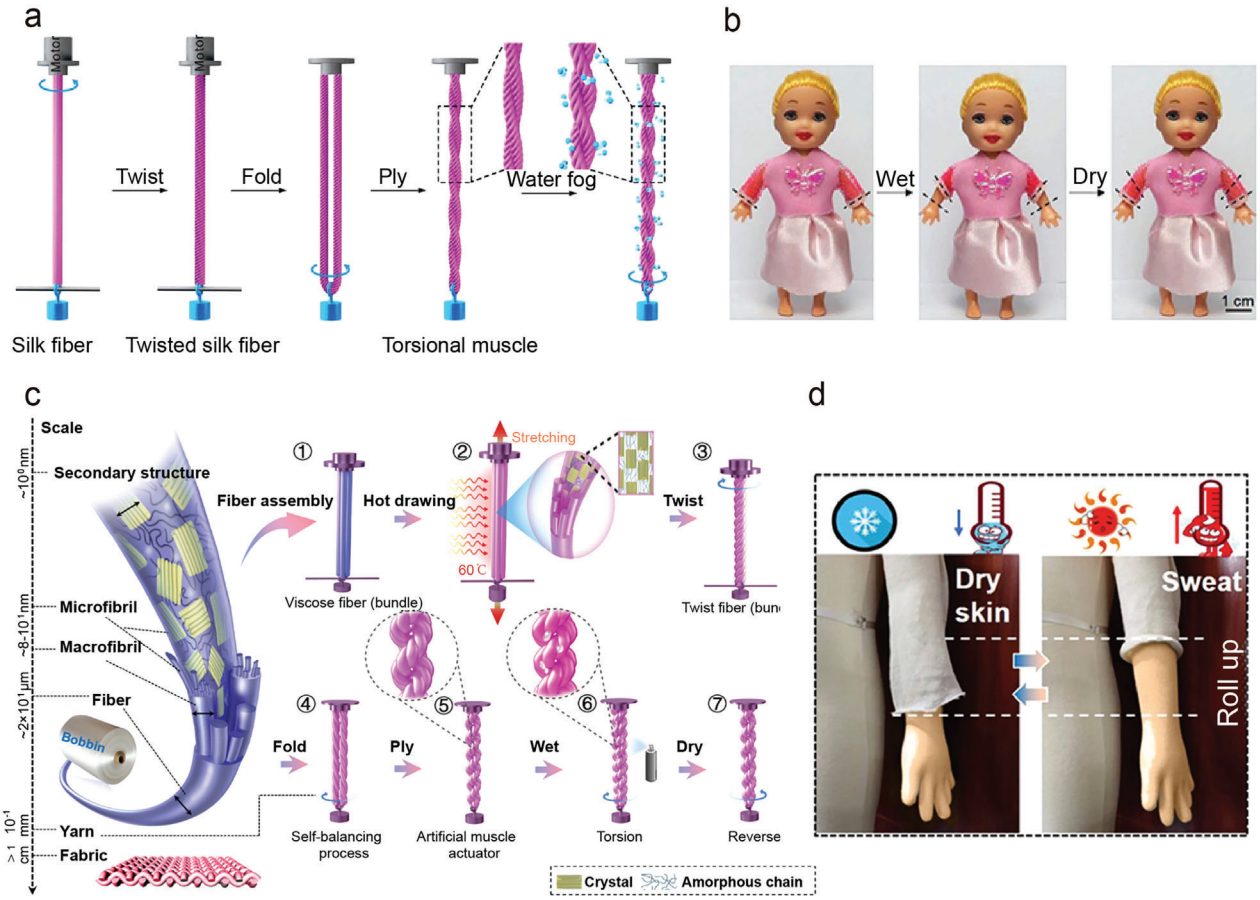

Figure 8. a) Schematic diagram of the production of silk two-layer torque-balanced torsion muscles. b) Photographs show smart-clothing sleeves contracting on exposure to moisture, and regaining their original length on exposure to dry air. a,b) Reproduced with permission.[47] Copyright 2019, Wiley-VCH. c) The cross-scale structure and basic manufacturing principles of viscose artificial muscles. d) Thermal management effects of garment sleeves in the dry-skin condition (left) and sweat-induced roll-up condition (right). c,d) Reproduced with permission.[51] Copyright 2021, American Chemical Society.

poly[2-(2-methoxyethoxy)ethoxyethyl methacrylate] (PMEO2MA) with a lower critical solution temperature (LCST) and poly[*N*,*N*-dimethyl(methacryloylethyl)ammonium propane sulfonate] (PDMAPS) with an upper critical solution temperature (UCST). The textile structure, consisting of upper and lower layers with channels, enables the construction of adaptive thermal-moisture management devices that are temperature-change dependent. At high temperatures, the lower-end diameter of the channel is larger than that of its upper end, and sweat is transferred from the hydrophobic LCST side to the hydrophilic UCST side for rapid evaporation, cooling the microclimate between the skin and textile. At low temperatures, the shape of the channel is reversed, effectively preserving heat and moisture in the microclimate to maintain warmth. As a result, under hot conditions, the structure exhibits 50% higher water evaporation and a temperature that is 1.2–2.3 °C lower than that shown by cotton textiles (Figure 10e); moreover, it exhibits a maximum temperature that is 3.3 °C higher than that exhibited by cotton textiles under cold conditions.

In addition to regulating moisture/sweat evaporation through textile design for thermal management of the human body, some studies have used power generation to construct multifunctional textiles.[70–71] Zhang et al.[70] have designed a breathable sandwich-structure material (PTFE/cobalt-complex-based super-hygroscopic material (Co-SHM)/PTFE) that enables the rapid evaporation of sweat to keep the human body in a dry state (**Figure 11**a). Co-SHM exhibits rapid absorption kinetics, a low desorption temperature (≈50 °C), and high water uptake (4.6 g g^{-1}) (Figure 11b). Under similar conditions, T-shirts with pads fabricated with the sandwich-structure material remain completely dry, whereas those without pads exhibit a visible sweat stain. Moreover, sweat can be transduced into energy via electrode reactions. As shown in Figure 11c, with Zn and Cu as electrodes and Co-SHM as the electrolyte, the following electrode reactions occur:

$$\text{Anodic}: Zn \rightarrow Zn^{2+} + 2e^- \quad (9)$$

$$\text{Cathodic}: 2H^+ + 2e^- \rightarrow H_2 \quad (10)$$

The sandwich-structure textile generates a power-density output of up to 0.11 mW cm^{-2} under 80% humidity (Figure 11d).

© 2023 The Authors. Advanced Materials published by Wiley-VCH GmbH

15214095, 0, Downloaded from https://onlinelibrary.wiley.com/doi/10.1002/adma.202209825 by University Of Chicago Library, Wiley Online Library on [25/07/2023]. See the Terms and Conditions (https://onlinelibrary.wiley.com/terms-and-conditions) on Wiley Online Library for rules of use; OA articles are governed by the applicable Creative Commons License

Table 3. Summary and comparison of moisture-responsive textiles based on sweat-evaporation regulation reported in the literature.

	Materials	Functions	Thermal management performances	Sweat evaporating regulation performances
Dai et al.[63]	Janus polyester/nitrocellulose textile embedded with a conical micropore array	Directional transport, Cooling	Compared to cotton textiles, it maintains the human body at a 2–3 °C higher temperature.	A directional transport index of 1246%.
Miao et al.[64]	Aligned polyurethane/boron nitride nanosheet fibers	Directional transport, Cooling	Compared to cotton textiles, it maintains the human body at a 1 °C higher temperature.	A water-transport index of 1072%, rapid water evaporation rate (0.36 g h^{-1}), and outstanding through plane (0.182 W m^{-1} K^{-1}) and in-plane (1.137 W m^{-1} K^{-1}) thermal conductivities.
Peng et al.[65]	Original fabric/Ag/cellulose fibers	Sweat transportation, Cooling	It shows an ≈3 °C cooling effect in the artificial sweating-skin test, while consuming less sweat than cotton textiles.	Compared to cotton, the skin power density is 3 times higher, with over 100% reduction in the water mass-gain ratio.
Hu et al.[66]	Bilayer nanoporous polyethylene membrane	Rapid water transportation, Cooling	It exhibits temperatures that are ≈2.6 and ≈1.0 °C lower than those exhibited by cotton textiles without/with perspiration.	No specific value given.
Wang et al.[67]	Poly[2-(2-methoxyethoxy)ethoxyethyl methacrylate]/poly[*N*,*N*-dimethyl(methacryloylethyl)ammonium propane sulfonate]	Directional transport, Cooling, Heating	Under hot conditions, the structure exhibits 50% higher water evaporation and lower temperatures (by 1.2–2.3 °C) compared to cotton textiles. Under cold conditions, it exhibits temperatures that are up to 3.3 °C warmer than those exhibited by cotton textiles.	No specific value given.
Hu et al. ([68]	PU fibrous membrane(PU-E)/MXene@polydopamine-PU Janus membrane	Directional transport, Cooling, Heating	Its temperature increases to ≈36 ± 1 °C within 200 s, which is higher than that of PU-E (≈32 °C) and the ambient temperature (≈28.3 °C).	Good flexibility, outstanding mechanical strength, and flame retardancy.
Xu et al.[69]	Ag nanopowder/non-woven	Fast evaporation rate, Heating	On applying a voltage of 5 V, the surface of the textile shows temperatures up to 76.1 °C.	A sheet resistance of 1.116 Ω^{-1} and ultrafast evaporation rate (3.42 g h^{-1}).
Zhang et al.[70]	PTFE/cobalt-complex-based superhygroscopic material (Co-SHM)/PTFE	Sweat evaporation (cooling), Power generation	-	A water uptake of 4.6 g g^{-1} and power density of up to 0.11 mW cm^{-2} under 80% humidity.
Gong et al.[71]	A ferroelectric-enhanced triboelectric evaporation textile that includes a ferroelectric-enhanced TENG (FETENG) and a directional moisture-wicking fabric (DMWF).	Directional transport, Cooling, Power generation	Compared to commercial insoles, it exhibits an 0.8 °C temperature-drop after 40 min of exercise.	An instantaneous output power of 135 W m^{-2} and surface moisture content of ≈0%

In contrast to this method of using electrode reactions to generate electrical energy, Gong et al.[71] have reported electricity generation by a ferroelectric-enhanced triboelectric evaporation textile using a triboelectric nanogenerator (TENG); under the action of ferroelectric fibers, the system shows an instantaneous output power of 135 W m^{-2}. Moreover, owing to pore size and wettability gradient differences, the textile causes directional sweat transport from hydrophobic to hydrophilic layers. The surface moisture content of the hydrophobic layer close to the skin is always 0%. On using this material for insoles, compared to commercial insoles, a 0.8 °C temperature-drop is observed after 40 min of exercise.

5. Outlooks

Moisture-responsive textiles represent a new technology that can regulate the human microenvironment and improve personal comfort. This technology is expected to revolutionize traditional textile technology and promote sustainable development. In this review, the background, limitations, progress, and scope of moisture-responsive textiles based on flap opening and closing, yarn/fiber deformation, and sweat-evaporation regulation have been summarized and discussed, highlighting textile design for personal thermoregulation.

Although the thermal-management performance of moisture

© 2023 The Authors. Advanced Materials published by Wiley-VCH GmbH

15214095, 0, Downloaded from https://onlinelibrary.wiley.com/doi/10.1002/adma.202209825 by University Of Chicago Library, Wiley Online Library on [25/07/2023]. See the Terms and Conditions (https://onlinelibrary.wiley.com/terms-and-conditions) on Wiley Online Library for rules of use; OA articles are governed by the applicable Creative Commons License

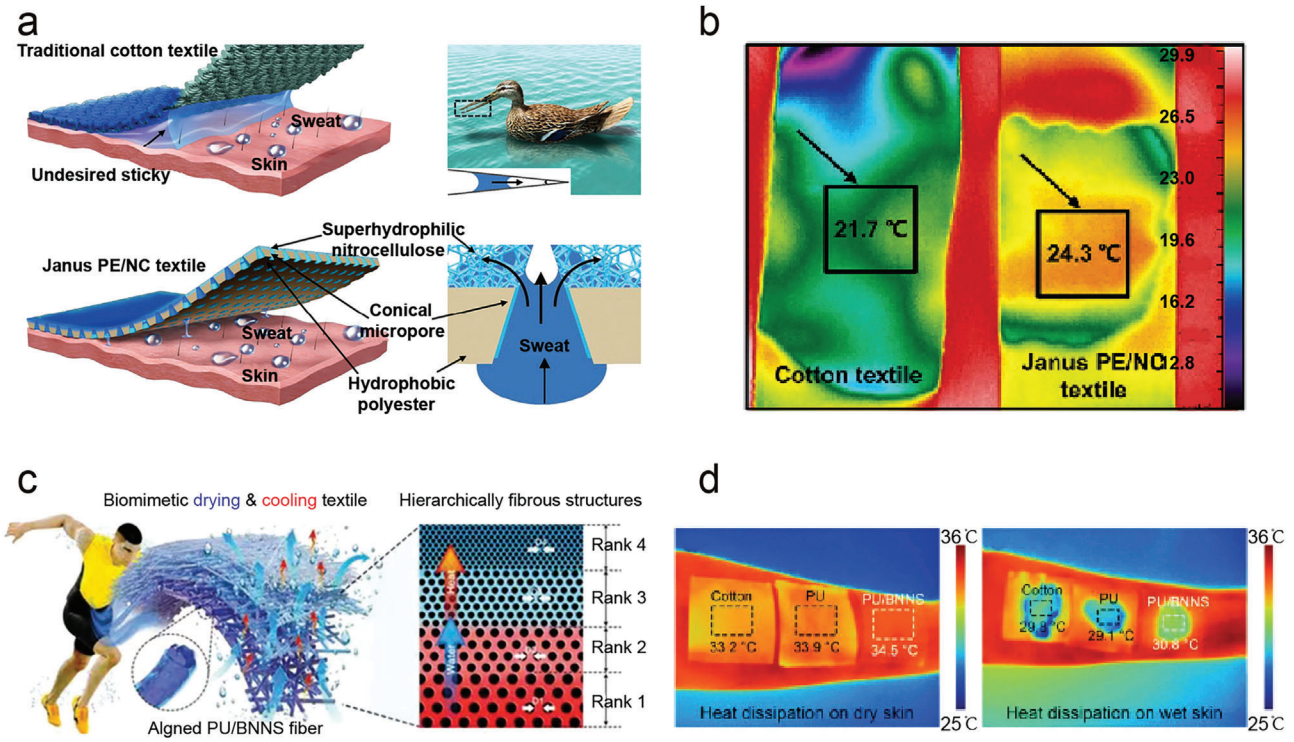

Figure 9. a) Schematic diagram showing capillary forces between conventional cotton fabric and wet skin (above). Schematic diagram of the human sweat-output path of skin covered with the Janus PE/NC textile with a tapered microporous design (below). b) IR pictures of Janus PE/NC and cotton textiles on moist skin. a,b) Reproduced with permission.[63] Copyright 2019, Wiley-VCH. c) Schematic illustration of the bionic multilayer fiber film as a personal drying and cooling functional textile for sweat release and heat dissipation; the right-hand-side inset shows a cross-section of the layered fiber structure. d) IR pictures of the heat dissipation performance of cotton textiles, PU multilayers, and PU/BNNS multilayers under dry and wet conditions. c,d) Reproduced with permission.[64] Copyright 2021, Wiley-VCH GmbH.

responsive textiles has improved significantly since their inception, some issues require resolution. The reported textiles exhibit significantly lower wearability, washability, and recyclability than traditional textiles; these features have not been considered systematically in the literature. Therefore, future studies should analyze these factors in detail.

First, some perspectives regarding moisture-responsive textiles based on flap opening and closing are discussed. Numerous high-performance (Nafion, microbial cells, etc.) and low-cost materials (nylon 6) have been reported for moisture-responsive textiles based on flap design. The coordinated regulation of evaporation, thermal radiation, thermal conduction, and convection has been reported for personal thermal management; however, the following limitations should be addressed. First, although hygroscopic materials show good cyclic properties in response to moisture, their cyclic performance decreases significantly for sweat wetting. Developing new materials with good cyclic performance under moisture and sweat infiltration, or avoiding sweat infiltration in the existing systems, may overcome this limitation. Second, for flap processing, direct cutting with razor blades tends to form small gaps between the flaps and base material, hindering flap switching. Therefore, it is vital to develop other controllable and scaled printing processes and patterning techniques.

Considering moisture-responsive textiles based on yarn/fiber deformation, numerous textiles with good performance have been reported. Some traditional-textile parameters, such as gas permeability, water permeability, and weaving, have also been considered for woolen systems. The stability and nontoxicity of textiles (some systems modulate the properties of textiles by adding nanomaterials) should be considered in future studies. Moreover, most studies analyze changes in textile properties, such as porosity and length, and very few have investigated the correlation between textile-structure changes and thermal regulation. Therefore, it is vital to quantitatively test the regulation temperature or heat-dissipation power of textiles. This could provide direct feedback for the future design and optimization of textile materials.

In sweat-evaporation regulation using textile design for personal thermoregulation, differences in hydrophilicity and hydrophobicity between the inner and outer surfaces of the textile and microstructure design have been used to facilitate the directional transport of sweat. Some studies have reported sweat-evaporation cooling during this process. However, efficient cooling through the design of textile materials and structures, heat transfer, and evaporation requires further investigation. Future studies should focus on increasing the evaporation rate by designing the outer surface of the textile for a greater cooling power and lower temperature drop, efficiently utilizing the outer-surface evaporation cooling for human-body cooling. These heat transfer and evaporation aspects may require research in the field of interfacial solar vapor generation.[72–81] Moreover, dynamic

 © 2023 The Authors. Advanced Materials published by Wiley-VCH GmbH

15214095, 0, Downloaded from https://onlinelibrary.wiley.com/doi/10.1002/adma.202209825 by University Of Chicago Library, Wiley Online Library on [25/07/2023]. See the Terms and Conditions (https://onlinelibrary.wiley.com/terms-and-conditions) on Wiley Online Library for rules of use; OA articles are governed by the applicable Creative Commons License

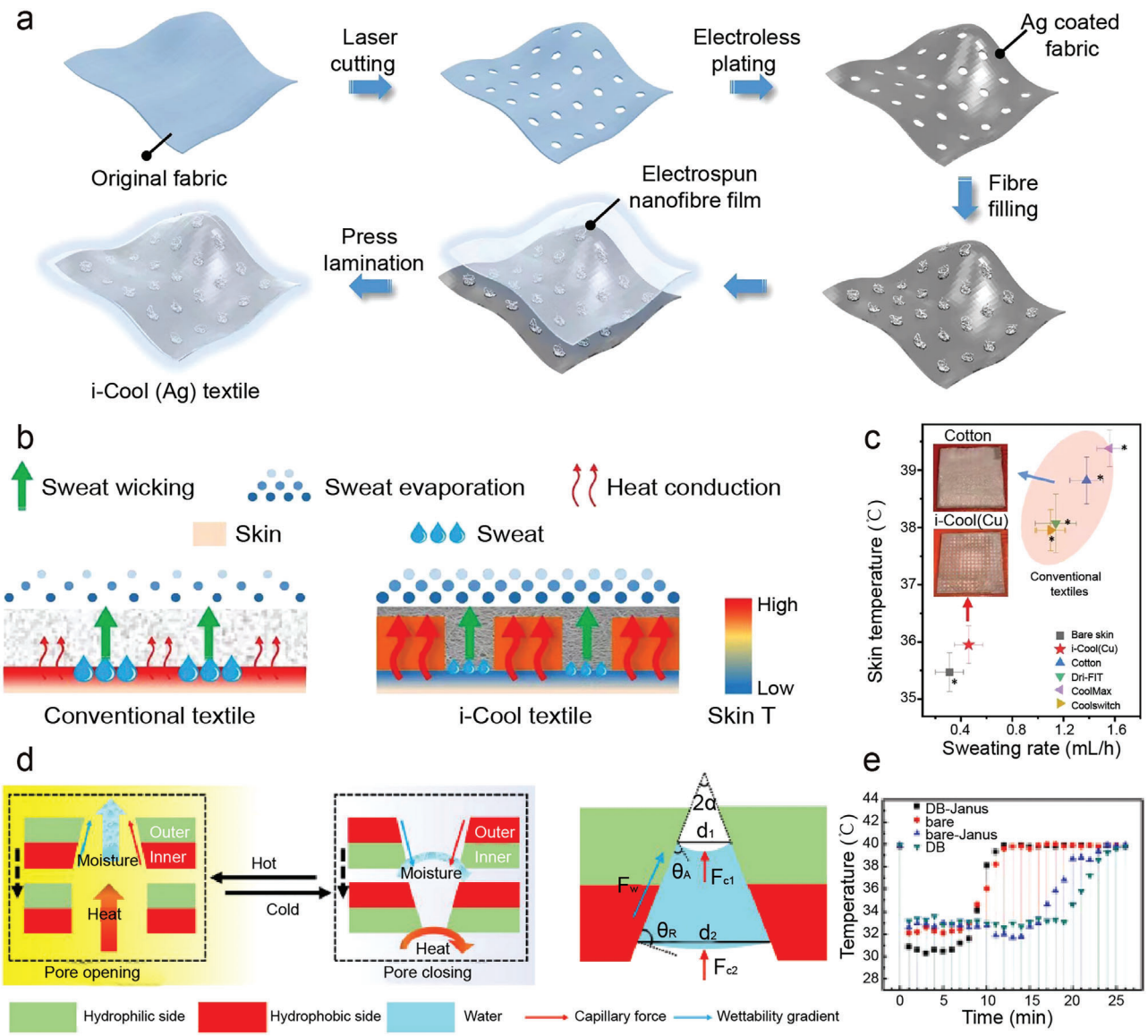

Figure 10. a) Illustration of the i-Cool (Ag) textile manufacturing process. b) Comparison of conventional and i-Cool textiles; the red arrow indicates differences in thermal conductivity. The dot size and density comparisons in the sweat evaporation graph show the different evaporation capacities. c) Skin temperature and sweating rate measurements on naked skin, and skin covered with i-Cool (Cu) and commercial textiles (skin power density: 750 W m^{-2}, ambient temperature: 22 °C). a–c) Reproduced with permission.[65] Copyright 2021, Springer Nature. d) The thermal-moisture management mechanism of the DB-Janus textile is based on a reversible moisture gradient and pore-size variation (left). The driving force of water droplets inside the DB-Janus fabric is shown on the right-hand side. e) Comparison of surface temperatures of the DB-Janus, bare cotton, bare Janus, and DB-cotton textiles during water evaporation at an ambient temperature of 40 °C. d,e) Reproduced with permission.[67] Copyright 2019, Wiley-VCH.

heating and cooling smart-materials with directional sweat transport have been recently developed. Future studies should focus on the development of high-performance materials and structures. Research on passive radiative cooling textiles involves sweat management to improve the textile comfort; it could be interesting to combine radiative and sweat-evaporation cooling for a high overall cooling power.

The use of sweat evaporation to combine power generation devices with textiles is an important branch in the research of smart textiles. However, the overall power generation by this method is currently low. Future research can combine hydrovoltaic technologies[82–89] and biofuel cells[90–96] for high power-generation efficiencies. Additionally, the collaboration of energy storage electronic/electric devices and other devices with smart textiles could enable personal thermal and energy management.

Summarizing, hygroscopic smart textiles have developed rapidly over the past few years; however, there is still a gap between lab-scale proof-of-concept devices and practical applications. This review will help researchers understand the current status of this field, with its bottlenecks, to overcome its limitations and promote practical applications in the near future.

© 2023 The Authors. Advanced Materials published by Wiley-VCH GmbH

15214095, 0, Downloaded from https://onlinelibrary.wiley.com/doi/10.1002/adma.202209825 by University Of Chicago Library, Wiley Online Library on [25/07/2023]. See the Terms and Conditions (https://onlinelibrary.wiley.com/terms-and-conditions) on Wiley Online Library for rules of use; OA articles are governed by the applicable Creative Commons License

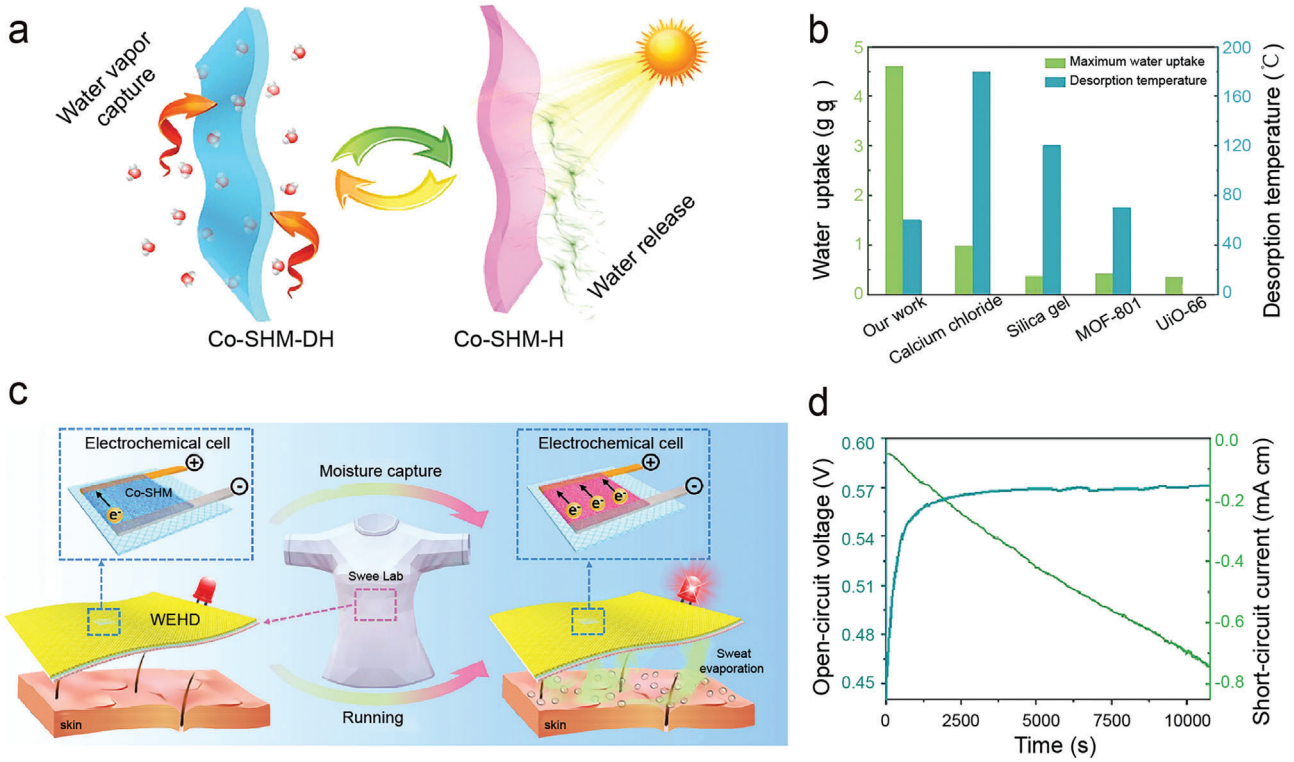

Figure 11. a) Schematic diagram of the water vapor absorption/desorption process. Co-SHM in the dehydrated state (Co-SHM-DH) traps water vapor and forms the hydrated state (Co-SHM-H). b) Comparison of the maximum water absorption and water desorption temperatures of several hygroscopic materials. c) Schematic diagram of the working regime of the proposed wearable energy harvesting device (WEHD). Each electrochemical cell contains Zn and Cu electrodes and Co-SHM as the electrolyte. d) The continuous open-circuit voltage and short-circuit current generated by an electrochemical cell with Co-SHM absorbing water vapor at 25 °C and 80% humidity. a–d) Reproduced with permission.[70] Copyright 2020, Elsevier.

Acknowledgements

This work was supported by the National Key Research and Development Program of China (2019YFA0705400), Natural Science Foundation of Jiangsu Province (BK20212008), Research Fund of State Key Laboratory of Mechanics and Control of Mechanical Structures (MCMS-I-0421K01, MCMS-I-0422K01), Fundamental Research Funds for the Central Universities (NJ2022002), Fund of Prospective Layout of Scientific Research for NUAA (Nanjing University of Aeronautics and Astronautics), and NUAA Startup Fund (4017-YQR22012). P.-C.H. acknowledges funding from the Pritzker School of Molecular Engineering, University of Chicago.

Conflict of Interest

The authors declare no conflict of interest.

Keywords

directional fluid transport, moisture-responsive materials, textiles, thermoregulation

Received: October 25, 2022
Revised: January 17, 2023
Published online:

[1] K. Leblanc, in *Laparoscopic Hernia Surgery: An Operative Guide*, CRC Press, Boca Raton, FL, USA **2002**.
[2] K. Min, Y. Son, C. Kim, Y. Lee, K. Hong, *Int. J. Heat Mass Transfer* **2007**, *50*, 5292.
[3] Y. Cui, H. Gong, Y. Wang, D. Li, H. Bai, *Adv. Mater.* **2018**, *30*, 1706807.
[4] P. C. Hsu, X. Liu, C. Liu, X. Xie, H. R. Lee, A. J. Welch, T. Zhao, Y. Cui, *Nano Lett.* **2015**, *15*, 365.
[5] A. Hazarika, B. K. Deka, D. Kim, H. E. Jeong, Y. B. Park, H. W. Park, *Nano Lett.* **2018**, *18*, 6731.
[6] Q. Liu, J. Huang, J. Zhang, Y. Hong, Y. Wan, Q. Wang, M. Gong, Z. Wu, C. F. Guo, *ACS Appl. Mater. Interfaces* **2018**, *10*, 2026.
[7] Z. Liang, Z. Zhou, J. Li, S. Zhang, B. Dong, L. Zhao, C. Wu, H. Yang, F. Chen, S. Wang, *Chem. Eng. J.* **2021**, *415*, 128980.
[8] B. Zhu, W. Li, Q. Zhang, D. Li, X. Liu, Y. Wang, N. Xu, Z. Wu, J. Li, X. Li, P. B. Catrysse, W. Xu, S. Fan, J. Zhu, *Nat. Nanotechnol.* **2021**, *16*, 1342.
[9] L. Cai, Y. Peng, J. Xu, C. Zhou, C. Zhou, P. Wu, D. Lin, S. Fan, Y. Cui, *Joule* **2019**, *3*, 1478.
[10] L. Cai, A. Y. Song, P. Wu, P. C. Hsu, Y. Peng, J. Chen, C. Liu, P. B. Catrysse, Y. Liu, A. Yang, C. Zhou, C. Zhou, S. Fan, Y. Cui, *Nat. Commun.* **2017**, *8*, 496.
[11] X. Li, W. Xie, C. Sui, P.-C. Hsu, *ACS Mater. Lett.* **2020**, *2*, 1624.
[12] L. M. Lozano, S. Hong, Y. Huang, H. Zandavi, Y. A. El Aoud, Y. Tsurimaki, J. Zhou, Y. Xu, R. M. Osgood, G. Chen, S. V. Boriskina, *Opt. Mater. Express* **2019**, *9*, 1990.

© 2023 The Authors. Advanced Materials published by Wiley-VCH GmbH

15214095, 0, Downloaded from https://onlinelibrary.wiley.com/doi/10.1002/adma.202209825 by University Of Chicago Library, Wiley Online Library on [25/07/2023]. See the Terms and Conditions (https://onlinelibrary.wiley.com/terms-and-conditions) on Wiley Online Library for rules of use; OA articles are governed by the applicable Creative Commons License

[13] Y. Peng, J. Chen, A. Y. Song, P. B. Catrysse, P.-C. Hsu, L. Cai, B. Liu, Y. Zhu, G. Zhou, D. S. Wu, H. R. Lee, S. Fan, Y. Cui, *Nat. Sustainability* **2018**, *1*, 105.
[14] J. K. Tong, X. Huang, S. V. Boriskina, J. Loomis, Y. Xu, G. Chen, *ACS Photonics* **2015**, *2*, 769.
[15] P.-C. Hsu, A. Y. Song, P. B. Catrysse, C. Liu, Y. Peng, J. Xie, S. Fan, Y. Cui, *Science* **2016**, *353*, 1019.
[16] Department of Energy, Heating and Cooling; www.energy.gov/heating-cooling (accessed: October 2022).
[17] T. Li, Y. Zhai, S. He, W. Gan, Z. Wei, M. Heidarinejad, D. Dalgo, R. Mi, X. Zhao, J. Song, *Science* **2019**, *364*, 760.
[18] D. Ürge-Vorsatz, O. Lucon, H. Akbari, P. Bertoldi, L. F. Cabeza, N. Eyre, A. Gadgil, D. Harvey, Y. Jiang, E. Liphoto, S. Mirasgedis, S. Murakami, J. Parikh, C. Pyke, M. Vilariño, in Climate Change 2014: Mitigation of Climate Change, Cambridge University Press, Cambridge, UK 2014, Ch. 9.
[19] A. Ghahramani, K. Zhang, K. Dutta, Z. Yang, B. Becerik-Gerber, *Appl. Energy* **2016**, *165*, 930.
[20] Y. Peng, Y. Cui, *Joule* **2020**, *4*, 724.
[21] P.-C. Hsu, X. Li, *Science* **2020**, *370*, 784.
[22] H. M. K. Ullah, J. Lejeune, A. Cayla, M. Monceaux, C. Campagne, É. Devaux, *Text. Res. J.* **2021**, *92*, 3351.
[23] K. Li, T. H. Chang, Z. Li, H. Yang, F. Fu, T. Li, J. S. Ho, P. Y. Chen, *Adv. Energy Mater.* **2019**, *9*, 1901687.
[24] D. J. Roach, C. Yuan, X. Kuang, V. C. Li, P. Blake, M. L. Romero, I. Hammel, K. Yu, H. J. Qi, *ACS Appl. Mater. Interfaces* **2019**, *11*, 19514.
[25] H. Fang, W. Xie, X. Li, K. Fan, Y. T. Lai, B. Sun, S. Bai, W. J. Padilla, P. C. Hsu, *Nano Lett.* **2021**, *21*, 4106.
[26] E. M. Leung, M. Colorado Escobar, G. T. Stiubianu, S. R. Jim, A. L. Vyatskikh, Z. Feng, N. Garner, P. Patel, K. L. Naughton, M. Follador, E. Karshalev, M. D. Trexler, A. A. Gorodetsky, *Nat. Commun.* **2019**, *10*, 1947.
[27] L. Peng, B. Su, A. Yu, X. Jiang, *Cellulose* **2019**, *26*, 6415.
[28] K. Rykaczewski, *Appl. Therm. Eng.* **2020**, *171*, 115122.
[29] Y. Zhong, F. Zhang, M. Wang, C. J. Gardner, G. Kim, Y. Liu, J. Leng, S. Jin, R. Chen, *Sci. Rep.* **2017**, *7*, 44208.
[30] J. Mu, G. Wang, H. Yan, H. Li, X. Wang, E. Gao, C. Hou, A. T. C. Pham, L. Wu, Q. Zhang, Y. Li, Z. Xu, Y. Guo, E. Reichmanis, H. Wang, M. Zhu, *Nat. Commun.* **2018**, *9*, 590.
[31] W. Wang, L. Yao, C.-Y. Cheng, T. Zhang, H. Atsumi, L. Wang, G. Wang, O. Anilionyte, H. Steiner, J. Ou, *Sci. Adv.* **2017**, *3*, e1601984.
[32] X. Li, B. Ma, J. Dai, C. Sui, D. Pande, D. R. Smith, L. C. Brinson, P.-C. Hsu, *Sci. Adv.* **2021**, *7*, eabj7906.
[33] V. Kapsali, J. Vincent, *Biomimetics* **2020**, *5*, 52.
[34] G. Kim, C. Gardner, K. Park, Y. Zhong, S. Jin, *Adv. Intell. Syst.* **2020**, *2*, 2000163.
[35] X. Yang, W. Wang, M. Miao, *ACS Appl. Mater. Interfaces* **2018**, *10*, 32256.
[36] H. Zhao, X. Qi, Y. Ma, X. Sun, X. Liu, X. Zhang, M. Tian, L. Qu, *Nano Lett.* **2021**, *21*, 8126.
[37] X. A. Zhang, S. Yu, B. Xu, M. Li, Z. Peng, Y. Wang, S. Deng, X. Wu, Z. Wu, M. Ouyang, *Science* **2019**, *363*, 619.
[38] K. Fu, Z. Yang, Y. Pei, Y. Wang, B. Xu, Y. Wang, B. Yang, L. Hu, *Adv. Fiber Mater.* **2019**, *1*, 61.
[39] J. Hu, M. Irfan Iqbal, F. Sun, *Adv. Funct. Mater.* **2020**, *30*, 2005033.
[40] M. I. Iqbal, F. Sun, B. Fei, Q. Xia, X. Wang, J. Hu, *ACS Appl. Mater. Interfaces* **2021**, *13*, 6298.
[41] H. Cheng, Y. Hu, F. Zhao, Z. Dong, Y. Wang, N. Chen, Z. Zhang, L. Qu, *Adv. Mater.* **2014**, *26*, 2909.
[42] C. S. Haines, N. Li, G. M. Spinks, A. E. Aliev, J. Di, R. H. Baughman, *Proc. Natl. Acad. Sci. USA* **2016**, *113*, 11709.
[43] S. He, P. Chen, L. Qiu, B. Wang, X. Sun, Y. Xu, H. Peng, *Angew. Chem., Int. Ed.* **2015**, *54*, 14880.
[44] X. Leng, X. Hu, W. Zhao, B. An, X. Zhou, Z. Liu, *Adv. Intell. Syst.* **2020**, *3*, 2000185.
[45] C. D. Onal, D. Rus, *Bioinspiration Biomimetics* **2013**, *8*, 026003.
[46] C. S. Haines, M. D. Lima, N. Li, G. M. Spinks, J. Foroughi, J. D. Madden, S. H. Kim, S. Fang, M. Jung de Andrade, F. Göktepe, *Science* **2014**, *343*, 868.
[47] T. Jia, Y. Wang, Y. Dou, Y. Li, M. Jung de Andrade, R. Wang, S. Fang, J. Li, Z. Yu, R. Qiao, Z. Liu, Y. Cheng, Y. Su, M. Minary-Jolandan, R. H. Baughman, D. Qian, Z. Liu, *Adv. Funct. Mater.* **2019**, *29*, 1808241.
[48] Z. Yin, S. Shi, X. Liang, M. Zhang, Q. Zheng, Y. Zhang, *Adv. Fiber Mater.* **2019**, *1*, 197.
[49] X. Hu, X. Leng, T. Jia, Z. Liu, *Chin. Phys. B* **2020**, *29*, 118103.
[50] X. Leng, X. Zhou, J. Liu, Y. Xiao, J. Sun, Y. Li, Z. Liu, *Mater. Horiz.* **2021**, *8*, 1538.
[51] Y. Peng, F. Sun, C. Xiao, M. I. Iqbal, Z. Sun, M. Guo, W. Gao, X. Hu, *ACS Appl. Mater. Interfaces* **2021**, *13*, 54386.
[52] Y. Wang, Z. Wang, Z. Lu, M. Jung de Andrade, S. Fang, Z. Zhang, J. Wu, R. H. Baughman, *ACS Appl. Mater. Interfaces* **2021**, *13*, 6642.
[53] A. A. Babar, D. Miao, N. Ali, J. Zhao, X. Wang, J. Yu, B. Ding, *ACS Appl. Mater. Interfaces* **2018**, *10*, 22866.
[54] G. Huang, X. Wei, Y. Gu, Z. Kang, L. Lao, L. Li, J. Fan, D. Shou, *Cell Rep. Phys. Sci.* **2022**, *3*, 100710.
[55] Y. Lin, C. Wang, D. Miao, N. Cheng, N. Meng, A. A. Babar, X. Wang, B. Ding, J. Yu, *ACS Appl. Mater. Interfaces* **2022**, *14*, 18944.
[56] D. Miao, Z. Huang, X. Wang, J. Yu, B. Ding, *Small* **2018**, *14*, 1801527.
[57] H. Wang, W. Wang, H. Wang, X. Jin, J. Li, Z. Zhu, *ACS Appl. Mater. Interfaces* **2018**, *10*, 32792.
[58] X. Wang, Z. Huang, D. Miao, J. Zhao, J. Yu, B. Ding, *ACS Nano* **2019**, *13*, 1060.
[59] Y.-Q. Xiao, C.-W. Kan, *Coatings* **2022**, *12*, 267.
[60] S. Yang, Z. Zhu, Z. Wu, J. Wu, K. Yin, *Appl. Phys. Lett.* **2020**, *117*, 213701.
[61] W. Zhou, X. Gong, Y. Li, Y. Si, S. Zhang, J. Yu, B. Ding, *Chem. Eng. J.* **2022**, *427*, 130925.
[62] L. Lao, D. Shou, Y. Wu, J. Fan, *Sci. Adv.* **2020**, *6*, eaaz0013.
[63] B. Dai, K. Li, L. Shi, X. Wan, X. Liu, F. Zhang, L. Jiang, S. Wang, *Adv. Mater.* **2019**, *31*, 1904113.
[64] D. Miao, X. Wang, J. Yu, B. Ding, *Adv. Funct. Mater.* **2021**, *31*, 2008705.
[65] Y. Peng, W. Li, B. Liu, W. Jin, J. Schaadt, J. Tang, G. Zhou, G. Wang, J. Zhou, C. Zhang, Y. Zhu, W. Huang, T. Wu, K. E. Goodson, C. Dames, R. Prasher, S. Fan, Y. Cui, *Nat. Commun.* **2021**, *12*, 6122.
[66] R. Hu, N. Wang, L. Hou, J. Liu, Z. Cui, C. Zhang, Y. Zhao, *ACS Appl. Mater. Interfaces* **2022**, *14*, 9833.
[67] Y. Wang, X. Liang, H. Zhu, J. H. Xin, Q. Zhang, S. Zhu, *Adv. Funct. Mater.* **2020**, *30*, 1907851.
[68] M. Hu, J. Wu, B. Tian, H. Pi, R. Wang, X. Zhang, *ACS Appl. Nano Mater.* **2022**, *5*, 7344.
[69] J. Xu, B. Xin, X. Du, C. Wang, Z. Chen, Y. Zheng, M. Zhou, *RSC Adv.* **2020**, *10*, 27512.
[70] X. Zhang, J. Yang, R. Borayek, H. Qu, D. K. Nandakumar, Q. Zhang, J. Ding, S. C. Tan, *Nano Energy* **2020**, *75*, 104873.
[71] W. Gong, X. Wang, W. Yang, J. Zhou, X. Han, M. D. Dickey, Y. Su, C. Hou, Y. Li, Q. Zhang, H. Wang, *Adv. Mater.* **2021**, *33*, 2007352.
[72] C. Chen, Y. Kuang, L. Hu, *Joule* **2019**, *3*, 683.
[73] X. Li, G. Ni, T. Cooper, N. Xu, J. Li, L. Zhou, X. Hu, B. Zhu, P. Yao, J. Zhu, *Joule* **2019**, *3*, 1798.
[74] X. Li, W. Xie, J. Zhu, *Adv. Sci.* **2022**, *9*, 2104181.
[75] Y. Pang, J. Zhang, R. Ma, Z. Qu, E. Lee, T. Luo, *ACS Energy Lett.* **2020**, *5*, 437.
[76] P. Tao, G. Ni, C. Song, W. Shang, J. Wu, J. Zhu, G. Chen, T. Deng, *Nat. Energy* **2018**, *3*, 1031.
[77] P. Zhang, Q. Liao, H. Yao, Y. Huang, H. Cheng, L. Qu, *Energy Storage Mater.* **2019**, *18*, 429.
[78] F. Zhao, Y. Guo, X. Zhou, W. Shi, G. Yu, *Nat. Rev. Mater.* **2020**, *5*, 388.

© 2023 The Authors. Advanced Materials published by Wiley-VCH GmbH

15214095, 0, Downloaded from https://onlinelibrary.wiley.com/doi/10.1002/adma.202209825 by University Of Chicago Library, Wiley Online Library on [25/07/2023]. See the Terms and Conditions (https://onlinelibrary.wiley.com/terms-and-conditions) on Wiley Online Library for rules of use; OA articles are governed by the applicable Creative Commons License

[79] L. Zhou, X. Li, G. W. Ni, S. Zhu, J. Zhu, *Natl. Sci. Rev.* **2019**, *6*, 562.
[80] L. Zhu, M. Gao, C. K. N. Peh, G. W. Ho, *Nano Energy* **2019**, *57*, 507.
[81] Z. Wang, T. Horseman, A. P. Straub, N. Y. Yip, D. Li, M. Elimelech, S. Lin, *Sci. Adv.* **2019**, *5*, eaax0763.
[82] S. Fang, J. Li, Y. Xu, C. Shen, W. Guo, *Joule* **2022**, *6*, 690.
[83] Y. Huang, H. Cheng, L. Qu, *ACS Mater. Lett.* **2021**, *3*, 193.
[84] J. Li, K. Liu, T. Ding, P. Yang, J. Duan, J. Zhou, *Nano Energy* **2019**, *58*, 797.
[85] L. Li, M. Hao, X. Yang, F. Sun, Y. Bai, H. Ding, S. Wang, T. Zhang, *Nano Energy* **2020**, *72*, 104705.
[86] Y. Qin, Y. Wang, X. Sun, Y. Li, H. Xu, Y. Tan, Y. Li, T. Song, B. Sun, *Angew. Chem., Int. Ed.* **2020**, *59*, 10619.
[87] G. Xue, Y. Xu, T. Ding, J. Li, J. Yin, W. Fei, Y. Cao, J. Yu, L. Yuan, L. Gong, J. Chen, S. Deng, J. Zhou, W. Guo, *Nat. Nanotechnol.* **2017**, *12*, 317.
[88] J. Yin, J. Zhou, S. Fang, W. Guo, *Joule* **2020**, *4*, 1852.
[89] Z. Zhang, X. Li, J. Yin, Y. Xu, W. Fei, M. Xue, Q. Wang, J. Zhou, W. Guo, *Nat. Nanotechnol.* **2018**, *13*, 1109.
[90] A. J. Bandodkar, I. Jeerapan, J. M. You, R. Nunez-Flores, J. Wang, *Nano Lett.* **2016**, *16*, 721.
[91] X. Chen, L. Yin, J. Lv, A. J. Gross, M. Le, N. G. Gutierrez, Y. Li, I. Jeerapan, F. Giroud, A. Berezovska, R. K. O'Reilly, S. Xu, S. Cosnier, J. Wang, *Adv. Funct. Mater.* **2019**, *29*, 1905785.
[92] W. Jia, G. Valdes-Ramirez, A. J. Bandodkar, J. R. Windmiller, J. Wang, *Angew. Chem., Int. Ed.* **2013**, *52*, 7233.
[93] C. H. Kwon, Y. Ko, D. Shin, M. Kwon, J. Park, W. K. Bae, S. W. Lee, J. Cho, *Nat. Commun.* **2018**, *9*, 4479.
[94] L. Manjakkal, L. Yin, A. Nathan, J. Wang, R. Dahiya, *Adv. Mater.* **2021**, *33*, 2100899.
[95] L. Yin, J.-M. Moon, J. R. Sempionatto, M. Lin, M. Cao, A. Trifonov, F. Zhang, Z. Lou, J.-M. Jeong, S.-J. Lee, S. Xu, J. Wang, *Joule* **2021**, *5*, 1888.
[96] J. Lv, G. Thangavel, Y. Li, J. Xiong, D. Gao, J. Ciou, M. W. M. Tan, I. Aziz, S. Chen, J. Chen, *Sci. Adv.* **2021**, *7*, eabg8433.

Xiuqiang Li is a professor at Nanjing University of Aeronautics and Astronautics in the Institute for Frontier Science. His lab focuses on hydrovoltaic materials and devices, nano-intelligent building materials and devices. Group website: http://www.nuaa-xiuqiangli-group.cn

Wanlin Guo is a Mechanicist, Academician of Chinese Academy of Sciences, Professor of Nanjing University of Aeronautics and Astronautics, President of Institute for Frontier Science. His lab focuses on nano-intelligent material devices, high-efficiency new energy conversion technology, brain-inspired intelligence, hydrology, 3D fatigue fracture and damage tolerance, structural durability design at high temperature.

Po-Chun Hsu is an assistant professor at University of Chicago in the Pritzker School of Molecular Engineering. His lab focuses on light and heat management, nanophotonic materials, energy sustainability, wearable technology, and carbon capture. His radiative cooling textile was selected as a one of the "Ten World-Changing Ideas" by Scientific American. Group website: https://pochunhsu.group/

© 2023 The Authors. Advanced Materials published by Wiley-VCH GmbH

15214095, 0, Downloaded from https://onlinelibrary.wiley.com/doi/10.1002/adma.202209825 by University Of Chicago Library, Wiley Online Library on [25/07/2023]. See the Terms and Conditions (https://onlinelibrary.wiley.com/terms-and-conditions) on Wiley Online Library for rules of use; OA articles are governed by the applicable Creative Commons License